ADVANCED MATERIALS

DOI: 10.1002/adma.200602972

Domain Control in Multiferroic $BiFeO_3$ through Substrate Vicinality**

By *Ying-Hao Chu*,* *Maria P. Cruz*, *Chan-Ho Yang*, *Lane W. Martin*, *Pei-Ling Yang*, *Jing-Xian Zhang*, *Kilho Lee*, *Pu Yu*, *Long-Qing Chen*, and *Ramamoorthy Ramesh*

Control over ferroelectric polarization variants in $BiFeO_3$ films through the use of various vicinal $SrTiO_3$ substrates is demonstrated. The ferroelectric polarization variants in these films are characterized by piezoelectric force microscopy and the corresponding structural variants are carefully analyzed and confirmed by X-ray diffraction. Implementation of this approach has given us the ability to create single domain $BiFeO_3$ films on (001), (110), and (111) surfaces. The piezo/ferroelectric properties of the $BiFeO_3$ films, in turn, can be tailored through this approach. Such results are very promising for continued exploration of $BiFeO_3$ films and provide a template for detailed multiferroic-coupling studies in the magnetoelectric $BiFeO_3$ system.

Magnetoelectric coupling in multiferroic materials has attracted much attention because of the intriguing science underpinning this phenomenon. Additionally, there is an exciting potential for applications and devices that take advantage of these materials with multiple order parameters.[1–4] $BiFeO_3$ (BFO) is a room temperature, single-phase magnetoelectric multiferroic with a ferroelectric Curie temperature of ~1103 K[5] and an antiferromagnetic Néel temperature of ~643 K.[6] Recent studies of BFO thin films have shown the existence of a large ferroelectric polarization, as well as a small net magnetization of the Dzyaloshinskii-Moriya type resulting from a canting of the antiferromagnetic sublattice.[7,8] The ferroelectric polarization in BFO can have orientations along the four cube diagonals (<111>), and the direction of the polarization can be changed by ferroelectric and ferroelastic switching.[9] Our previous studies have shown coupling between ferroelectricity and antiferromagnetism in BFO thin films resulting from the coupling of both antiferromagnetic and ferroelectric domains to the underlying ferroelastic domain switching events.[10] Such a study was a crucial first step in the exploration of approaches to control and manipulate magnetic properties using an electric field.

It was also noted, however, that these films exhibit a very complicated domain structure, which complicates the interpretation of the fundamental properties of this system as well as the interactions across hetero-interfaces. The lack of large single crystals of the desired crystallographic orientation provokes another motivation to explore approaches to create "single crystalline" epitaxial films that are free of ferroelectric/ferroelastic domains. Recent studies have explored the ability to control the ferroelectric domain configuration, which is formed after the phase transformation, through substrate engineering.[11,12] In this study, we demonstrate an approach to control the ferroelectric domain structure in BFO films through the use of vicinal $SrTiO_3$ (STO) substrates. This has enabled us to create thin films that "mimic" the primary crystal facets of the pseudo-cubic unit cell, namely single domain (100), (110), and (111) surfaces.

The ferroelectric domain structure of an epitaxial BFO film on STO substrates with different orientations can be modeled using the phase-field method[13] in which the spatial distribution of the polarization field and its evolution is described by the time dependent Ginzburg–Landau (TDGL) equations.[14] For a BFO film grown on a (001)-oriented perovskite substrate, there are eight possible ferroelectric polarization directions corresponding to the four structural variants of the rhombohedral phase (Fig. 1a). In this case, the individual domains are energetically degenerate, and domain structures with twinning are expected in order to relax the elastic energy of the film.[15] Experimentally, however, only the downward directed polarization variants are observed, indicating the existence of a self-poling effect (as a consequence of the bottom electrode). Figure 1b shows an in-plane (IP) piezoforce microscopy (PFM) image of a BFO film grown on (001) STO substrate. The three contrast levels observed in the IP-PFM images acquired along the two orthogonal <110> directions, together with the uniform out-of-plane (OP) PFM contrast (not shown), indicate that the domain structure of the BFO films is characterized by four polarization variants.[16] The

[*] Dr. Y.-H. Chu, Dr. M. P. Cruz, Dr. C.-H. Yang, L. W. Martin, P.-L. Yang, Dr. K. Lee, P. Yu, Prof. R. Ramesh
Department of Materials Science and Engineering &
Department of Physics, University of California
Berkeley, CA 94720 (USA)
E-mail: yhchu@lbl.edu
Dr. M. P. Cruz
Universidad Nacional Autónoma de México
Centro de Ciencias de la Materia Condensada
Km 107 Caretera Tijuana-Ensenada
Ensenada, B.C., C.P. 22800 (Mexico)
J.-X. Zhang, Prof. L.-Q. Chen
Department of Materials Science and Engineering
Pennsylvania State University
University Park, PA 16802 (USA)

[**] This work is supported by the Director, Office of Basic Energy Sciences, Materials Sciences Division of the US Department of Energy under contract DE-AC02-05CH11231 and an ONR-MURI grant No. E-21-6RU-G4. This work is also supported by the Korea Research Foundation Grant funded by the Korean Government (MOEHRD) (KRF-2005-214-D00302)

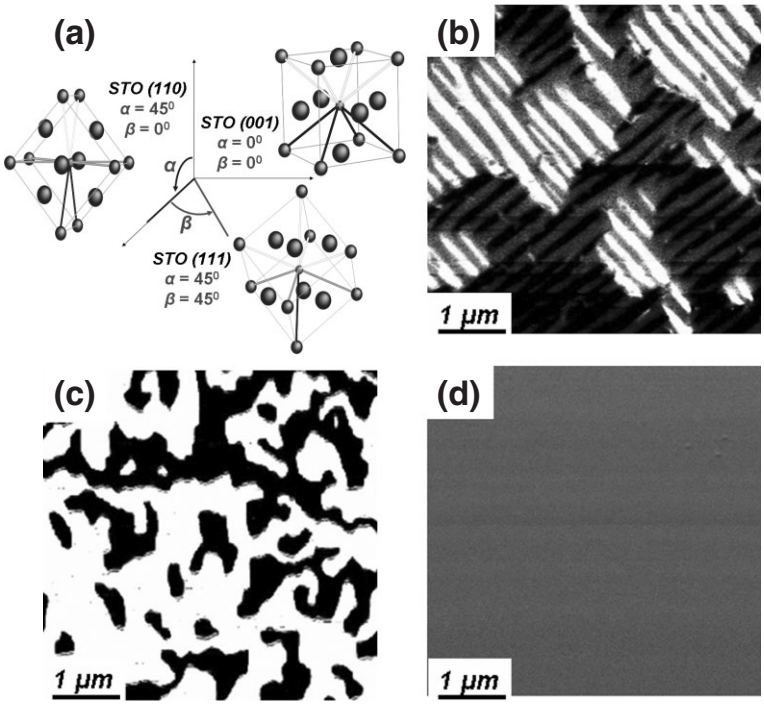

Figure 1. a) Schematic system of vicinal STO substrates and corresponding predicted polarization variants on STO(001), (110), and (111) substrates. IP-PFM images of BFO ferroelectric domain structures on b) STO (001), c) (110), and d) (111) substrates.

twin-wall orientations for stripe-like domains match well with those predicted from the phase-field simulation.

In the case of a film on an STO(110) substrate the relatively smaller substrate lattice parameter compressively strains the BFO film and causes the structure to favor four of the eight polarization variants. Since they have exactly the same spontaneous deformation on the (110) plane, the twin-structure formed by those variant pairs does not change the magnitude of the elastic energy; therefore, these twin boundaries are thermodynamically unstable and are not expected to exist in films grown on STO (110) substrates. However, as the growth temperature is lower than the Curie temperature and the self-poling effect, there is no selection for a particular polarization variant. Figure 1c shows the ferroelectric domain structure of BFO films grown on STO (110) substrates, (imaged with the cantilever along [1–10]), exhibiting only two ferroelectric variants with net polarization pointing down over large areas. Finally for growth on an STO(111) substrate, the polarization variants perpendicular to the film surface have the lowest energy for films grown under compressive strain. The stable domain structure in this case, therefore, is a single domain with a downward directed polarization. We have verified the domain structure of the BFO films grown on STO (111) substrates and, as anticipated, these films exhibited only one contrast in the out-of-plane (OP) (not shown) PFM image and no contrast for IP PFM image (Fig. 1d), suggesting the polarization direction of the films on STO (111) is perpendicular to the substrate. The key question then is how does one control the domain structures in Figure 1b and c such that they evolve into a single domain state as in Figure 1d?

In order to further control the domain structure of the BFO films, a break in symmetry of the ferroelectric variants is necessary. This is accomplished through the use of vicinal STO substrates, which effectively tilt and break the surface symmetry of the polarization variants. This is illustrated in Figure 1a for the case of the nominally (100) substrate. We use two parameters, α and β, to represent the vicinal angle and direction respectively. Figure 2a–c shows atomic force microscopy (AFM) images of typical vicinal STO substrates with different miscut angles. From the AFM images, the terrace width is observed to decrease with increasing vicinal angle. The corresponding PFM images of the subsequently grown BFO films are shown in Figure 2e–g. With only a 0.5° vicinal angle along the [010], the domain structure of the BFO films exhibit mainly two polarization variants which confirms that the ferroelectric symmetry can be broken through the use of vicinal substrates (Fig. 2f). Moreover, stripe patterns, created by two polarization variants 71° apart with polarization vectors pointing into the substrate, can also be observed (Fig. 2f). The width of these stripe domains has been measured over a

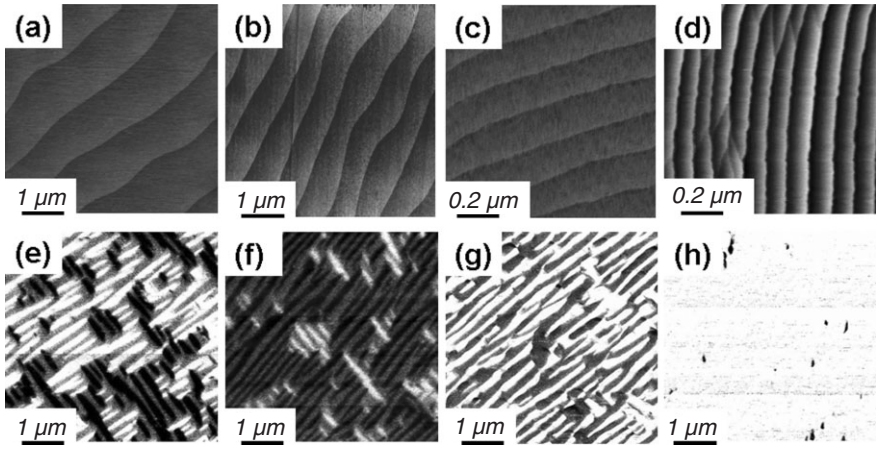

Figure 2. AFM images of typical vicinal STO substrates with different miscut angle [a) $\alpha = 0°$ and $\beta = 0°$, b) $\alpha = 0.5°$ and $\beta = 0°$, c) $\alpha = 1°$ and $\beta = 0°$, and d) $\alpha = 3°$ and $\beta = 45°$], and the corresponding IP-PFM images of BFO films [e) $\alpha = 0°$ and $\beta = 0°$, f) $\alpha = 0.5°$ and $\beta = 0°$, g) $\alpha = 1°$ and $\beta = 0°$, and h) $\alpha = 3°$ and $\beta = 45°$].

ADVANCED MATERIALS

number of samples to be ~200 nm; it is controlled, in part, by the film thickness. The long-axis of the stripe domains is parallel to the long direction of the terrace, suggesting the crucial role of the terrace width in determining the final domain structure. Our studies show that when the vicinal angle is small (i.e., less than 0.5°), with the corresponding terrace spacing > 1 μm, the film exhibits essentially equal fractions of the two sets of domains, suggesting that the domain formation is insensitive to such small vicinal angles. As the vicinal angle is increased to about 0.5°, Figure 2b, the fraction of domains that are perpendicular to the steps diminishes dramatically, Figure 2f, and at vicinal angles above 1°, Figure 2c, the film consists of essentially one set of domains, Figure 2g. Further changes in the vicinal angle do not change the domain architecture. Electrostatic forces and the minimization of elastic energy of the local stresses at step edges cause a break in symmetry from two sets of stripe domains to one set of stripe domains. Therefore, when the vicinal angle is increased, one set of stripe domains is more energetically favorable.

In order to apply the same approach to further simplify the domain structure in this orientation, we employ the second vicinal angle, with the miscut along the <110> ($\beta = 45°$) to induce the formation of one dominant ferroelectric variant. For example, on an STO (001) substrate with miscut angles of $\alpha = 3°$ and $\beta = 45°$ (Fig. 2d), we observe a uniform contrast in the PFM image of the BFO layer, indicating the formation of a monodomain architecture (Fig. 2h). Careful piezoforce imaging studies of this sample along various in-plane directions as well as with electrical poling further confirm the single domain nature.

X-ray scattering studies have been used to verify the domain architecture in these samples. In case of films grown on STO(001), the isotropic in-plane compressive strain from the STO substrate reduces the rhombohedral symmetry (R3c) of bulk BFO to monoclinic, which has been used as our structural model.[17,18] In this monoclinic structure (tilted along [–1–10]), the peak positions of the (203) and (023) reciprocal lattice reflections are shifted upward along the *L*-direction and by contrast the positions of (–203) and (0–23) are shifted downward. We symbolize the four possible monoclinically distorted structures as $M_{[110]}$, $M_{[-110]}$, $M_{[1-10]}$, $M_{[-1-10]}$, respectively, Figure 3a. Based on this model, we measured

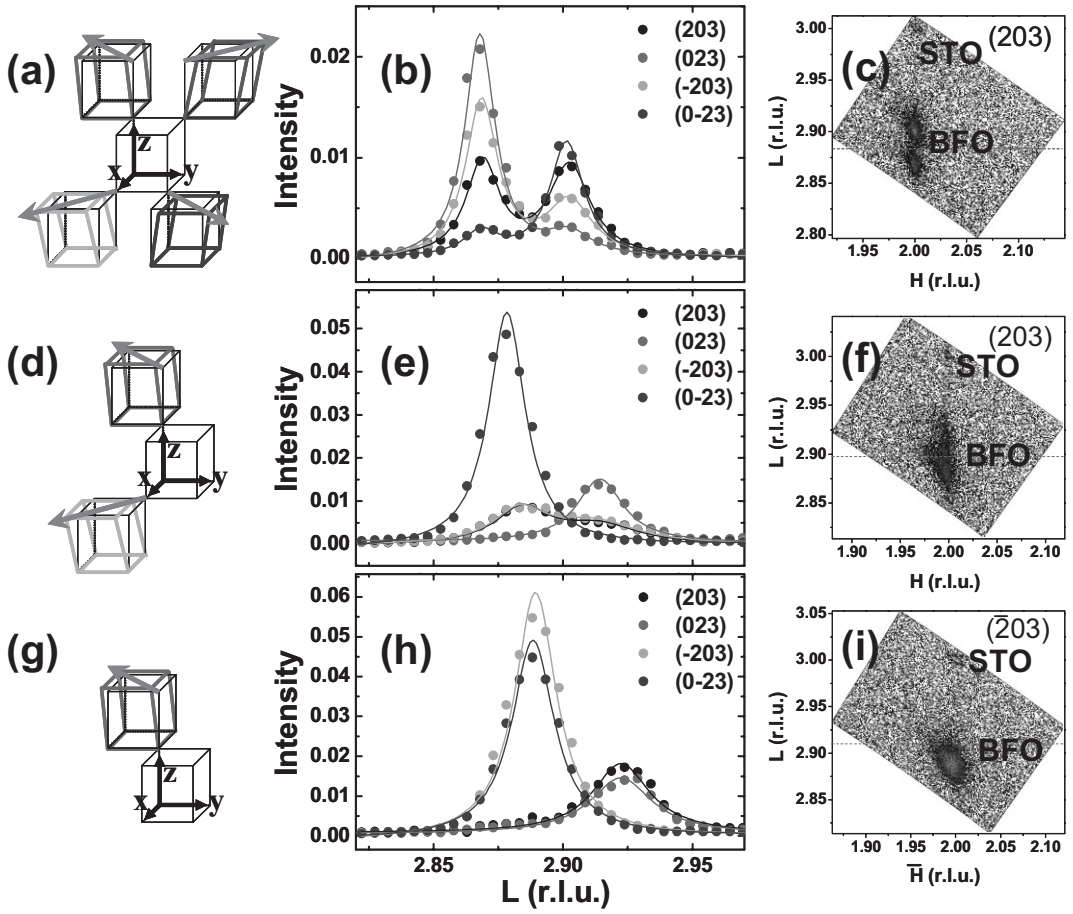

Figure 3. Schematic of the structure variants with a) four polarization variants, d) two polarization variants, and g) one polarization variant. The details for the {203} line scan and RSM results of BFO/SRO film grown on STO substrates with b)–c) four polarization variants, e)–f) two polarization variants, and (h–i) one polarization variant.

line scans along the L-direction in (HKL) reciprocal space mapping (RSM) for the (203), (023), (–203), and (0–23) reflections. These were selected to be a fingerprint for the four structural variants. All reciprocal space units are normalized to those of STO(1/0.3905 nm^{-1}). Figure 3a, d, and g are structure schematics for BFO films with different polarization variants. The films with four polarization variants show peak splitting for all {203} diffraction peaks (Fig. 3b and c), confirming the structure model. For the films with two polarization variants, peak-splitting was seen on the (203), while no peak splitting was observed on (023) (Fig. 3e and f), suggesting only two structural variants. Finally, the films with only one polarization variant displayed no peak-splitting (Fig. 3h and i). These findings are consistent with the results from the PFM images. Moreover, by calculating the splitting distance between two peaks, we can identify the monoclinic distortion angle to be ~0.7° along the [110].

The same approach can be applied to BFO films grown on STO(110). The two-domain architecture in the BFO(110) films (Fig. 4a) can likewise be controlled and evolve into a singledomain film on the STO(110) surface (Fig. 4b). The similar monoclinic structure model is also introduced in this orientation[19] (Fig. 4c and d). Therefore, RSMs have been used to further confirm the domain architecture in these samples. In this orientation, the peak positions of the (221) reciprocal lattice reflections were used as a fingerprint for the structural variants. For the films with two polarization variants, peak-splitting was seen on the (221) (Fig. 4e), suggesting only two structural variants. By contrast, the films with only one polarization variant displayed no peak-splitting (Fig. 4f). These findings are consistent with the results from the PFM images.

Quantitative OP piezoelectric response measurements (Fig. 5) reflect the systematic changes in domain populations; the remnant d_{33} value for the fully clamped BFO films increases from 30 pm V^{-1} to 60 pm V^{-1} as the number of ferroelectric polarization variants is increased. Such an enhancement is attributed to an extrinsic contribution from domain wall motion, which is evident if we compare the domain structure of the BFO films. Furthermore, the single domain films in the three orientations show essentially the same piezoelectric response (within the limits of the experimental observations).

In summary, we have demonstrated an elegant and systematic approach to control the domain variants in BFO thin

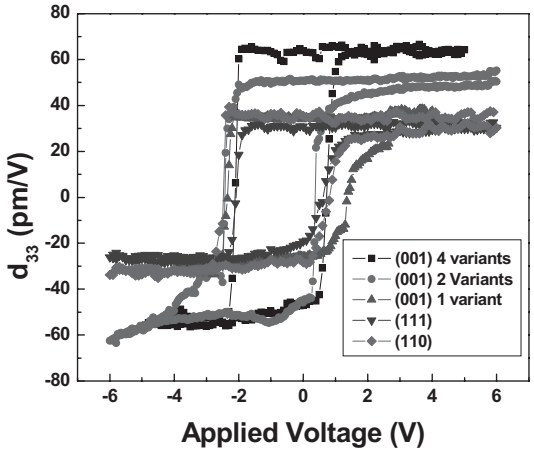

Figure 5. Piezoelectric hystersis loops, d_{33}-V, of BFO/SRO films on different vicinal STO substrates.

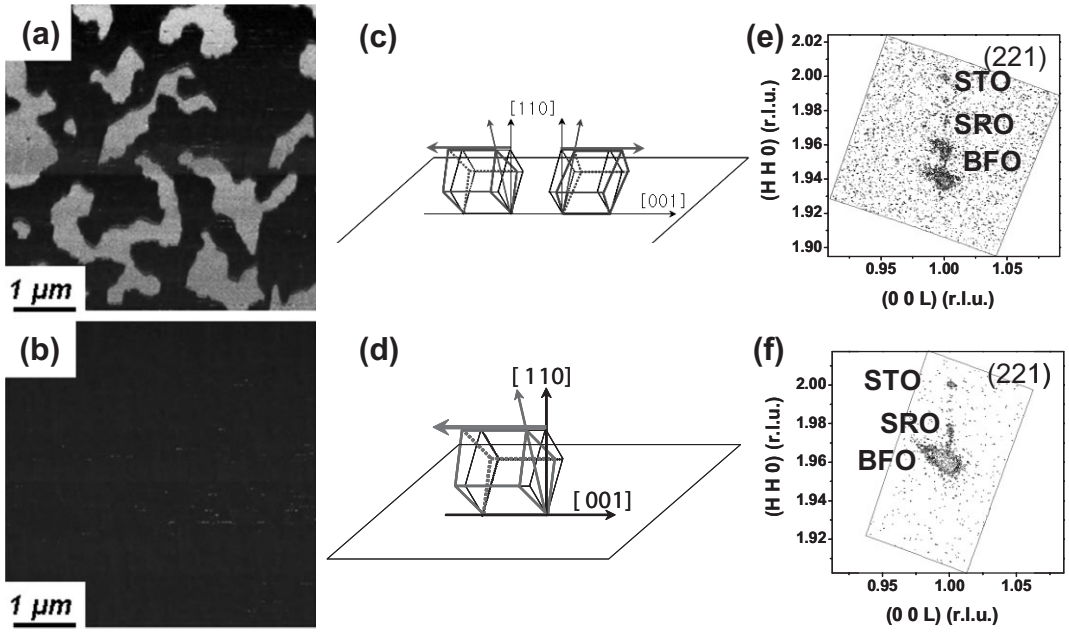

Figure 4. IP-PFM images of BFO ferroelectric domain structures on STO(110): a) two polarization variants and b) one polarization variant. Schematic of the structure variants with c) two polarization variants, and d) one polarization variants on STO(110). The RSM results of BFO/SRO film grown on STO(110) substrates with (c) two polarization variants, and (d) one polarization variant.

ADVANCED MATERIALS

films using substrate vicinality as the critical control parameter. Implementation of this approach on (100) and (110) STO substrates has given us the ability to create single domain BFO films on such surfaces. This, in conjunction with the fact that epitaxial films on (111) STO with an SRO bottom electrode also exhibit a single domain behavior, provides us with set of model thin film systems to further explore the magnetoelectric properties of this system as well as its interactions with other layers (such as a ferromagnet).

Experimental

Commercially available STO (001) substrates with vicinal miscut of varying degrees along <010> and <110> were used for this study. For each growth the substrates were etched by buffered HF and annealed in air at 1000 °C for 2 h to achieve an optimum terraced morphology [20,21]. A thin (~40 nm), pseudomorphic layer of SRO deposited by pulsed laser deposition (PLD) was used as a bottom electrode for the BFO films. Films of 100–120 nm thick BFO were deposited over the SRO layer by PLD at 700 °C and 100 mTorr of oxygen. The crystallinity of the BFO/SRO/STO films was studied by x-ray diffraction. Reciprocal space mapping (RSM) was performed using a Philips X'Pert PRO X-ray Diffraction System. Pt/SRO top electrodes (32 μm in diameter) were patterned in order to measure the piezoelectric properties. Morphology and local piezoelectric properties were investigated using an atomic force microscope (AFM)-based setup [16].

Received: December 28, 2006
Revised: April 13, 2007
Published online: August 21, 2007

[1] R. Ramesh, N. A. Spaldin, *Nat. Mater.* **2007**, *6*, 21.
[2] W. Eerenstein, N. D. Mathur, J. F. Scott, *Nature* **2006**, *422*, 759.
[3] N. A. Spaldin, M. Fiebig, *Science* **2005**, *309*, 391.
[4] M. Fiebig, T. Lottermoser, D. Frohlich, A. V. Goltsev, R. V. Pisarev, *Nature* **2002**, *419*, 818.
[5] G. A. Smolenskii, V. Isupov, A. Agranovskaya, N. Kranik, *Sov. Phys.–Solid State* **1961**, *2*, 2651.
[6] P. Fischer, M. Polomska, I. Sosnowska, M. Szymanski, *J. Phys. C* **1980**, *13*, 1931.
[7] J. Wang, J. B. Neaton, H. Zheng, V. Nagarajan, S. B. Ogale, B. Liu, D. Viehland, V. Vaithyanathan, D. G. Schlom, U. V. Waghmare, N. A. Spaldin, K. M. Rabe, M. Wuttig, R. Ramesh, *Science* **2003**, *299*, 1719.
[8] C. Ederer, N. A. Spaldin, *Phys. Rev. B* **2005**, *71*, 060 401(R).
[9] F. Kubel, H. Schmid, *Acta Crystallogr. Sect. B* **1990**, *46*, 698.
[10] T. Zhao, A. Scholl, F. Zavaliche, K. Lee, M. Barry, A. Doran, M. P. Cruz, Y. H. Chu, C. Ederer, N. A. Spaldin, R. R. Das, D. M. Kim, S. H. Baek, C. B. Eom, R. Ramesh, *Nat. Mater.* **2006**, *5*, 823.
[11] V. Nagarajan, C. S. Ganpule, H. Li, L. Salamanca-Riba, A. L. Roytburd, E. D. Williams, R. Ramesh, *Appl. Phys. Lett.* **2001**, *79*, 2805.
[12] Y. H. Chu, Q. Zhan, L. W. Martin, M. P. Cruz, P. L. Yang, G. W. Pabst, F. Zavaliche, S. Y. Yang, J. X. Zhang, L. Q. Chen, D. G. Schlom, I. Nan. Lin, T. B. Wu, R. Ramesh, *Adv. Mater.* **2006**, *18*, 2307.
[13] J. X. Zhang, L. Q. Chen, unpublished.
[14] L. Q. Chen, *Annu. Rev. Mater. Res.* **2002**, *32*, 113.
[15] S. K. Streiffer, C. B. Parker, A. E. Romanov, M. J. Lefevre, L. Zhao, J. S. Speck, W. Pompe, C. M. Foster, G. R. Bai, *J. Appl. Phys.* **1998**, *83*, 2742.
[16] F. Zavaliche, S. Y. Yang, T. Zhao, Y. H. Chu, M. P. Cruz, R. Ramesh, *Phase Transitions* **2006**, *79*, 991.
[17] J. Li, J. Wang, M. Wuttig, R. Ramesh, N. Wang, B. Ruette, A. P. Pyatakov, A. K. Zvevdin, D. Vielhand, *Appl. Phys. Lett.* **2004**, *84*, 5261.
[18] G. Xu, H. Hiraka, G. Shirane, J. F. Li, J. Wang, D. Viehland, *Appl. Phys. Lett.* **2005**, *86*, 182 905.
[19] G. Xu, J. Li, D. Viehland, *Appl. Phys. Lett.* **2006**, *89*, 222 901.
[20] M. Kawasaki, K. Takahashi, T. Maeda, R. Tsuchiya, M. Shinohara, O. Ishiyama, T. Yonezawa, M. Yoshimoto, H. Koinuma, *Science* **1994**, *266*, 1540.
[21] T. Ohnishi, K. Shibuya, M. Lippmaa, D. Kobayashi, H. Kumigashira, M. Oshima, H. Koinuma, *Appl. Phys. Lett.* **2004**, *85*, 272.

